Mech Time-Depend Mater
https://doi.org/10.1007/s11043-020-09448-y

# Nanoindentation measurement of core–skin interphase viscoelastic properties in a sandwich glass composite

**Dongyang Cao[1] · Sadeq Malakooti[1] · Vijay N. Kulkarni[1] · Yao Ren[1] · Hongbing Lu[1]**

Received: 25 November 2019 / Accepted: 15 April 2020


**Abstract** Debonding at the core–skin interphase region is one of the primary failure modes in core sandwich composites under shear loads. As a result, the ability to characterize the mechanical properties at the interphase region between the composite skin and core is critical for design analysis. This work intends to use nanoindentation to characterize the viscoelastic properties at the interphase region, which can potentially have mechanical properties changing from the composite skin to the core. A sandwich composite using a polyvinyl chloride foam core covered with glass fiber/resin composite skins was prepared by vacuum-assisted resin transfer molding. Nanoindentation at an array of sites was made by a Berkovich nanoindenter tip. The recorded nanoindentation load and depth as a function of time were analyzed using viscoelastic analysis. Results are reported for the shear creep compliance and Young's relaxation modulus at various locations of the interphase region. The change of viscoelastic properties from higher values close to the fiber composite skin region to the smaller values close to the foam core was captured. The Young's modulus at a given strain rate, which is also equal to the time-averaged Young's modulus across the interphase region was obtained. The interphase Young's modulus at a loading rate of 1 mN $s^{-1}$ was determined to change from 1.4 GPa close to composite skin to 0.8 GPa close to the core. This work demonstrated the feasibility and effectiveness of nanoindentation-based interphase characterizations to be used as an input for the interphase stress distribution calculations, which can eventually enrich the design process of such sandwich composites.

**Keywords** Sandwich composite · Core–skin interphase · Berkovich tip · Viscoelastic nanoindentation

Dongyang Cao and Sadeq Malakooti contributed equally to this work.

✉ H. Lu
hongbing.lu@utdallas.edu

[1] Department of Mechanical Engineering, The University of Texas at Dallas Richardson, TX 75080, USA

Published online: 30 April 2020

## 1 Introduction

Lightweight, cost-effective, and high strength sandwich composites have become the material of choice for wind turbine blades in the wind power industry (Brøndsted et al. 2005). Most commonly, those composites are composed of glass fiber skins bonded to a foam core such as polyvinyl chloride core through a wet lay-up or a vacuum-assisted resin transfer molding (VARTM) process (Chen et al. 2017; Dai and Hahn 2003; Stewart 2009). It has been well established that the high bonding strength at the core–skin interphase region dictates crack growth retardation and fatigue life improvement of sandwich composites under service conditions (Frostig 1992). However, the mechanical properties at interphase, which is typically spanned over a few hundred microns filled with polymeric resins, can be highly complex and time-dependent. For that reason, typical mechanical experiments at bulk scales are not capable to quantitatively characterize the mechanical properties at the interphase region. In an attempt to address this issue, the focus of the current study will be on the nanoindentation measurement of the local viscoelastic properties including creep compliance and Young's relaxation modulus as a function of time at the interphase region between the core and the skin of a sandwich composite.

The interest in the nanoindentation measurements of polymer viscoelastic properties has gained attention primarily for the purpose of materials characterization using a small amount of materials (Huang and Lu 2006, 2007; Jakes et al. 2012; Lu et al. 2003; Kucuk et al. 2013). While there are some indentation-based studies on the characterization of the interphase region in fiber-reinforced polymer matrix composites, e.g. (Cech et al. 2013; Gibson 2014), to the best of our knowledge, the attempts on characterizing the mechanical properties at the interphase region of sandwich composites are very limited and the viscoelastic effects are not considered, e.g. (Du and Jiao 2009; Flores-Johnson and Li 2011; Rizov et al. 2005). It is noted that the use of viscoelastic nanoindentation analysis is necessary for polymers as the Oliver–Pharr indentation approach (Oliver and Pharr 1992) is not suitable for viscoelastic solids due to issues including rate dependency of the unloading slope and the presence of nose, or bulge effect at the beginning of the unloading part of a nanoindentation load–displacement curve (Briscoe et al. 1998; Feng and Ngan 2002; Liu et al. 2006; Ngan et al. 2005; Ngan and Tang 2002).

Accordingly, following a viscoelastic nanoindentation approach previously developed (Lu et al. 2003), the time-dependent properties of the core–skin interphase region of a glass fiber–PVC foam sandwich composite were investigated. Specifically, using a Berkovich nanoindenter tip at a constant loading rate, the nanoindentation load–displacement curves at an array of grid points in the interphase region were obtained. Subsequently, the creep compliance was determined, and then it was converted to Young's relaxation modulus as a functions of time at the interphase region. Finally, the spatial variations of the averaged Young's modulus across the interphase region were studied.

## 2 Experiments

The materials and sample preparation, along with details of the nanoindentation measurements, are described in this section.

### 2.1 Materials and sample preparation

The sandwich composite sample was fabricated through a vacuum-assisted resin transfer molding (VARTM) process (Chen et al. 2017). Epoxy resin (Epikote$^{TM}$ MGS$^{TM}$ 135; Hexion, Inc., Columbus, OH) and curing agent (Epikure$^{TM}$ MGS$^{TM}$ RIMH 1366; Hexion, Inc.,

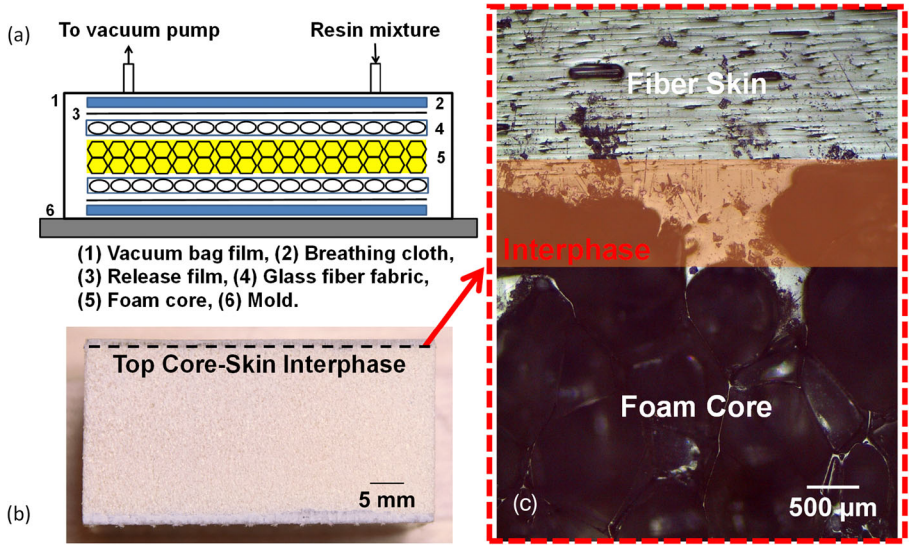


**Fig. 1** (**a**) Schematic of the VARTM setup; (**b**) The cross-section of the glass fiber PVC–foam sandwich composite; (**c**) An optical micrograph of an interphase region between the foam core and the fiber skin of the sandwich composite sample

Columbus, OH) were mixed (10:3 w/w) at room temperature. Unidirectional glass fiber fabrics (UD 970; Saertex, LLC, Huntersville, NC) with a surface density of 957 g/m$^2$ and a nominal thickness of 1 mm were used as the face-sheet material. Two breathing cloths (Polyester; FibreGlast, Brookville, OH), and two release films (Fluorinated ethylene propylene; FibreGlast, Brookville, OH) were also used in the VARTM process. The use of a breather is necessary to reach an even vacuum distribution across the entire surface of the laminate. PVC foams (Divinycell™ H60; Diab Group, Helsingborg, Sweden) were used as the core material. The foams were cut using a waterjet cutter to a nominal thickness of 25.4 mm. Then, the cores, before use, were cleaned with ethanol (Fisher Chemical, Lawn, NJ) and dried for 1 h under room conditions. The schematic of the VARTM setup is shown in Fig. 1(a).

The composite skins were made of 2 layers of the glass fiber fabrics on each side. Next, one side of the mold was sprayed with a release agent (MRTM 311; Sprayon, Cleveland, OH) and then, breathing cloth, release film, glass fiber fabric, PVC foam, glass fiber fabric, release film, and breathing cloth were laid in order (see Fig. 1(a)). Later, the entire laminate was covered by a vacuum bag film (Nylon; FibreGlast, Brookville, OH) and sealed with a sealant tape (Yellow tape; FibreGlast, Brookville, OH). Then, the epoxy resin mixture (previously degassed at 40 °C for 30 min) was transferred to the laminate. Next, the vacuum was applied for 2 h until the epoxy mixture was infiltrated the entire sandwich structure at room temperature. Finally, the vacuum-bagged sandwich composite was placed in an oven for three curing steps, initially at 45 °C, then at 55 °C, and finally at 65 °C, each for 4 h.

## 2.2 Nanoindentation measurement

The nanoindentation experiments were carried out at room temperature. Nanoindentation specimen was taken from a rectangular piece of the sandwich composite (Fig. 1(b)) using

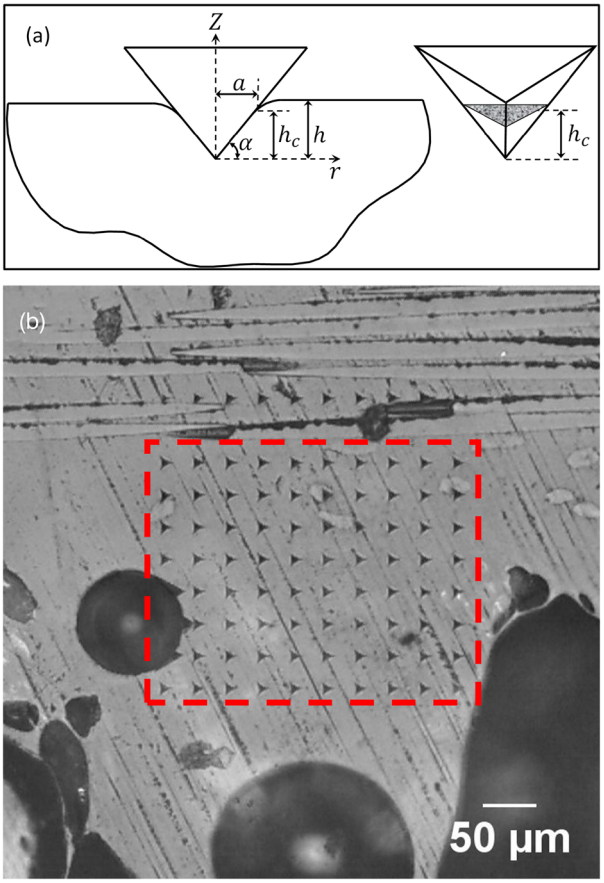


**Fig. 2** (**a**) Schematic of Berkovich indentation; (**b**) The optical micrograph of the residual indents bounded with a dashed red-color square containing $8 \times 10$ grid locations with 30 μm spacing (Color figure online)

a high-speed diamond cut-off saw (MTI Corp., Richmond, CA). The surface was prepared for nanoindentation on the cross-section of the sample (containing a part of the glass fiber skin, the interphase region and a part of the foam core) using an automated polisher (NANO 1000T polisher; Pace Technologies, Tucson, AZ), check Fig. 1(c).

An Agilent G200 Nano Indenter with a Berkovich diamond tip was used for nanoindentation measurements on the interphase region of the sandwich composite. The schematic of a Berkovich indentation is shown in Fig. 2(a). The indenter can reach a maximum indentation depth of 500 μm (0.2 nm resolution) and a maximum load of 500 mN (50 nN resolution). A maximum load of 20 mN was applied on the indenter tip with a constant loading rate of 1 mN/s. The nanoindentation measurements were repeated at several points across the interphase region containing $8 \times 10$ grid locations with a 30 μm spacing (Fig. 2(b)).

## 3 Viscoelastic nanoindentation analysis

Following the theory of linear viscoelasticity (Ferry 1980) and Sneddon's solution (Sneddon 1965), the corresponding author previously developed a viscoelastic nanoindentation approach for solid polymers (Lu et al. 2003). A brief background of the method is explained

in the following. Here, we consider a rigid Berkovich indenter tip (shown in Fig. 2(a)) indenting a linearly viscoelastic, isotropic, and homogenous half-space with a constant rate loading history of $F(t) = \dot{F}_0 t H(t)$, where $t$ is the elapsed time, $\dot{F}_0$ is the constant loading rate, and $H(t)$ is the Heaviside unit step function. Under these conditions and considering the generalized Kelvin model, the indentation displacement $h(t)$ can be written as follows (Huang 2007):

$$h^2(t) = \frac{\pi(1-\upsilon)}{4\cot(\alpha)} \left\{ \left( J_0 + \sum_{i=1}^{N} J_i \right) F(t) - \sum_{i=1}^{N} J_i \left( \dot{F}_0 \tau_i \right) \left( 1 - e^{-F(t)/F_0 \tau_i} \right) \right\}, \tag{1}$$

where $\alpha$ is the angle between the cone generator and the substrate plane, $\upsilon$ is the Poisson's ratio (which is herein assumed to be constant and equal to 0.3), $J_0$ and $J_i$ ($i = 1, 2, \ldots, N$) are shear creep coefficients, and $\tau_i$ ($i = 1, 2, \ldots, N$) are retardation times. Then, fitting Eq. (1) over an experimental nanoindentation load–displacement curve will determine the shear creep coefficients, the retardation times, and subsequently the creep function based on the generalized Kelvin model as $J(t) = J_0 + \sum_{i=1}^{N} J_i \left(1 - e^{-t/\tau_i}\right)$. Next, the relaxation function based on the generalized Maxwell model, $E(t) = E_\infty + \sum_{i=1}^{N} E_i e^{-t/\lambda_i}$, where $E_\infty$ and $E_i$ ($i = 1, 2, \ldots, N$) are relaxation coefficients, and $\lambda_i$ ($i = 1, 2, \ldots, N$) are relaxation times can be determined using the Volterra equation (Ferry 1980),

$$\int_0^t E(\zeta) J(t-\zeta) d\zeta = 2(1+\upsilon)t. \tag{2}$$

It is worth mentioning that special attention should be made on the quality of creep compliance data for the very short times due to the fact that Eq. (2) is an ill-posed problem, e.g. (Baumgaertel and Winter 1989; Emri and Tschoegl 1993; Tschoegl et al. 1992). Lastly, Young's modulus at a strain rate which is equal to the time-average Young's relaxation modulus $\overline{E}(t)$ can be obtained using $\overline{E}(t) = \frac{\sigma(t)}{\varepsilon(t)} = \frac{1}{t}\int_0^t E(\zeta) d\zeta$. A short time should be chosen for the lower bound of the integral in order to construct a dependable experimental data.

## 4 Results and discussion

In order to characterize the viscoelastic properties at the interphase region, nanoindentation was carried out at the $8 \times 10$ grid locations as shown in Fig. 2(b) and schematically in the inset of Fig. 3. Here, the viscoelastic properties were extracted from the loading part of the nanoindentation load–displacement curve. Therefore, only the loading curves of the nanoindentation load-displacement results were shown in Fig. 3. Each nanoindentation load–displacement curve in Fig. 3 is the average of nanoindentation load–displacement curves obtained from each grid row. Since the measurements were load-controlled, the displacements were continuously recorded for the prescribed load history. All nanoindentation loading curves were continued up to 20 mN maximum force. Figure 3 inherently shows a gradient in stiffness at the interphase as the maximum displacement at 20 mN maximum load in the load-displacement curves are shifting from right (softer at the core side) to left (stiffer at the skin side). The percentage change in the creep compliances from the core side (grid row = 1) to the skin side (grid row = 8) at time 19 s is 22%.

A nonlinear least-squares fit can be obtained on each spatially averaged nanoindentation curve to determine the creep coefficients and retardation times. However, it has been shown

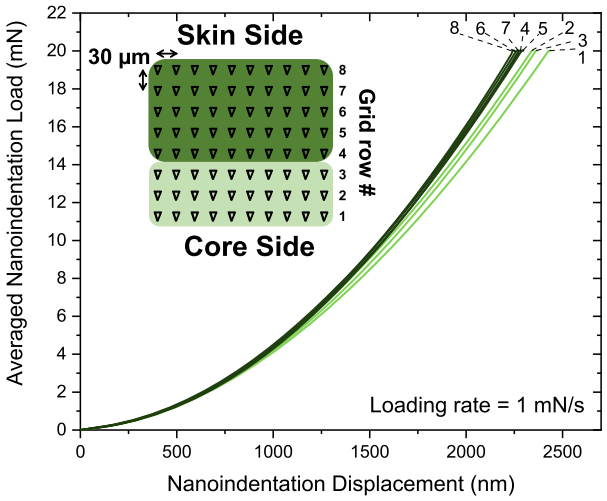


**Fig. 3** Spatial-averaged nanoindentation load–displacement curves at the core–skin interphase region of the sandwich composite using a Berkovich indenter tip. The schematic of the indented area and positions is also shown in the inset

**Table 1** Creep compliance coefficients based on the generalized Kelvin model at different interphase locations obtained through a nonlinear least squares fitting technique

| Grid row # | The generalized Kelvin model based creep compliance coefficients (1/GPa) | | | | |
|---|---|---|---|---|---|
| | $J_0$ | $J_1$ | $J_2$ | $J_3$ | $J_4$ |
| 1 | 0.119 | 0.178 | 0.559 | 0.452 | 0.303 |
| 2 | 0.116 | 0.173 | 0.558 | 0.386 | 0.280 |
| 3 | 0.174 | 0.212 | 0.498 | 0.385 | 0.225 |
| 4 | 0.163 | 0.194 | 0.433 | 0.396 | 0.210 |
| 5 | 0.219 | 0.237 | 0.376 | 0.404 | 0.136 |
| 6 | 0.229 | 0.244 | 0.359 | 0.387 | 0.111 |
| 7 | 0.266 | 0.275 | 0.353 | 0.363 | 0.078 |
| 8 | 0.260 | 0.268 | 0.328 | 0.369 | 0.065 |

that the use of one retardation time per decade is normally acceptable (Knauss and Zhao 2007). Here, four predetermined retardation times were chosen (0.01 s, 0.1 s, 1 s, and 10 s). The corresponding compliance coefficients $J_i$ were then obtained from the fitting process. A typical least squares correlation coefficient of $1 \times 10^{-5}$, indicating a good correlation, was obtained. The compliance coefficients determined by fitting for each grid row are listed in Table 1.

Using the obtained compliance coefficients, the average shear creep compliance function at each grid row as a function of time was determined and plotted in Fig. 4. The long-term shear creep compliance values are generally decreasing at the interphase region towards the skin side in agreement with our previous nanoindentation observations. This reduction is essentially due to the glass fiber adhesion effects on the local properties of the resin at the skin side of the interphase region.

The Young's relaxation function based on the generalized Maxwell model can be then acquired using Eq. (2) and the obtained shear creep compliance functions, through another nonlinear least square fitting process. The relaxation modulus coefficients and times are listed in Tables 2 and 3, respectively.

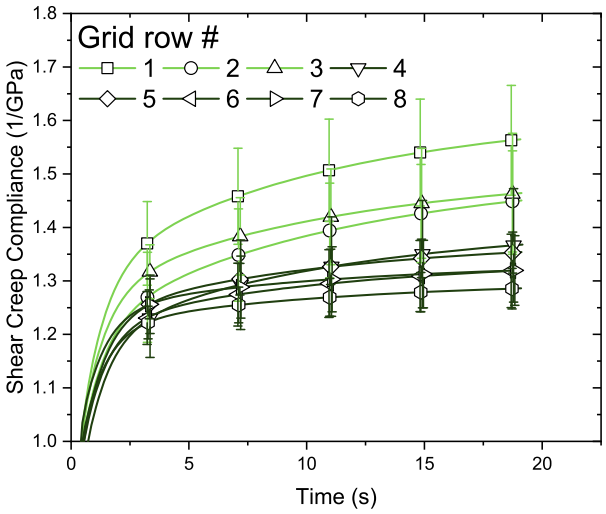


**Fig. 4** Spatial-averaged shear creep compliance curves as a function of time at different interphase grid rows from nanoindentation measurements

**Table 2** Relaxation modulus coefficients based on the generalized Maxwell model at different interphase locations obtained through a nonlinear least squares fitting technique

| Grid row # | The generalized Maxwell model based Young's relaxation coefficients (GPa) | | | | |
|---|---|---|---|---|---|
| | $E_\infty$ | $E_1$ | $E_2$ | $E_3$ | $E_4$ |
| 1 | 0.623 | $1.49 \times 10^8$ | 0.958 | 0.399 | 0.070 |
| 2 | 0.667 | $6.45 \times 10^9$ | 1.023 | 0.507 | 0.079 |
| 3 | 0.673 | $1.98 \times 10^8$ | 1.067 | 0.410 | 0.108 |
| 4 | 0.721 | $4.27 \times 10^8$ | 1.148 | 0.399 | 0.115 |
| 5 | 0.730 | 2.311 | 1.288 | 0.374 | 0.141 |
| 6 | 0.745 | 2.074 | 1.363 | 0.385 | 0.148 |
| 7 | 0.751 | 1.288 | 1.373 | 0.416 | 0.181 |
| 8 | 0.776 | 1.040 | 1.523 | 0.408 | 0.187 |

**Table 3** Relaxation times based on the generalized Maxwell model at different interphase locations obtained through a nonlinear least squares fitting technique

| Grid row # | The generalized Maxwell model based relaxation times (s) | | | |
|---|---|---|---|---|
| | $\lambda_1$ | $\lambda_2$ | $\lambda_3$ | $\lambda_4$ |
| 1 | $5.45 \times 10^8$ | 1.983 | 0.163 | 0.011 |
| 2 | $2.41 \times 10^{10}$ | 1.912 | 0.176 | 0.011 |
| 3 | $1.02 \times 10^9$ | 1.949 | 0.159 | 0.012 |
| 4 | $2.12 \times 10^9$ | 2.024 | 0.153 | 0.012 |
| 5 | 18.087 | 2.096 | 0.146 | 0.012 |
| 6 | 16.892 | 2.148 | 0.146 | 0.012 |
| 7 | 14.201 | 2.052 | 0.147 | 0.013 |
| 8 | 13.161 | 2.142 | 0.145 | 0.013 |

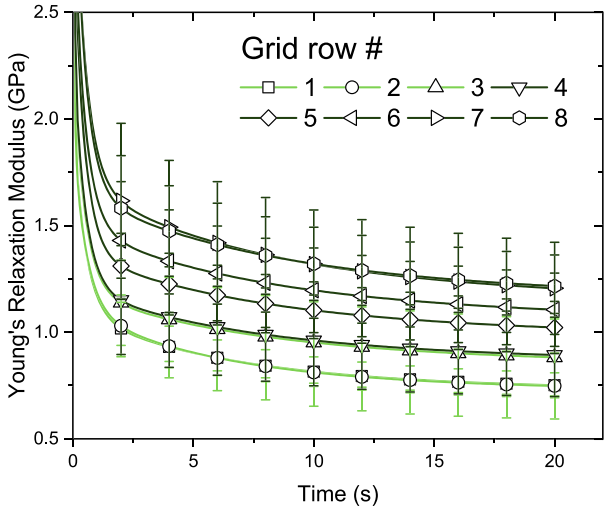


**Fig. 5** Spatial-averaged Young's relaxation modulus curves as a function of time at different interphase grid rows from nanoindentation measurements

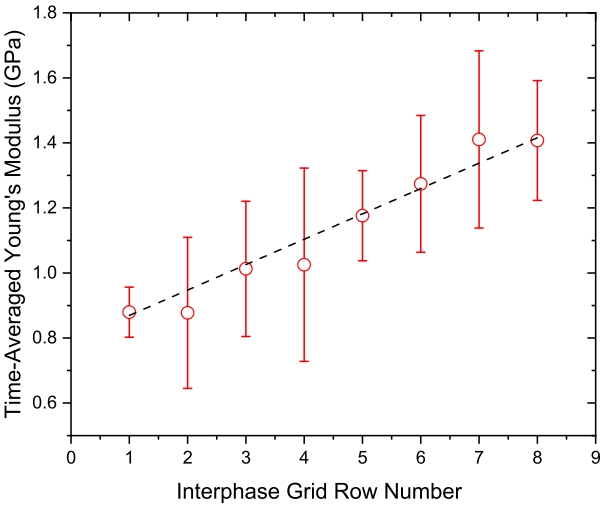


**Fig. 6** Time-averaged Young's modulus at different interphase grid rows from nanoindentation measurements

Figure 5 shows the obtained Young's relaxation functions at different grid rows. The long-term Young's relaxation modulus of the interphase at the vicinity of the fiber side is become more than doubled due to the fiber adhesion effects (the percentage change in the Young's relaxation modulus from the core side, grid row = 1, to the skin side, grid row = 8, at time 20 s is 62%).

The Young's modulus at a given strain rate of $10^{-5}$ $s^{-1}$, which is equal to the time-averaged Young's modulus across the interphase region (using results from the Young's relaxation modulus curves, Fig. 5) can provide insight on the variation of the stiffness at the interphase from the core to skin. Figure 6 shows the time-averaged Young's modulus (over 20 s time interval) at different interphase grid locations. These measurements show that the interphase region was stiffened significantly across its interphase thickness from PVC foam to fiber skin. This dramatic change in modulus is measured across a very short distance

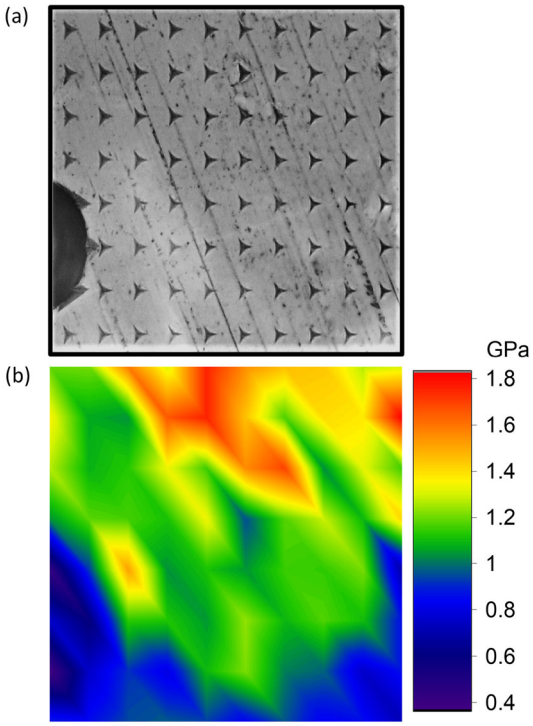


**Fig. 7** Spatial variation of the average Young's modulus at the interphase region: (**a**) optical micrograph of residual indents from $8 \times 10$ nanoindentations by Berkovich tip on the core–skin interphase region of the sandwich composite; (**b**) Spatial distribution of average Young's modulus in the same area shown in (a) (Color figure online)

(240 μm) which indicates the effectiveness of this approach for the interphase mechanical characterization.

In order to have a better understanding on the variation of the mechanical properties at the interphase, the spatial variation of the time-averaged Young's modulus over the entire indented area against its optical micrograph is shown in Fig. 7. The presence of void imperfection in the nanoindentation grid area (as it can be seen for example in the lower-left corner of the optical image) can be traced with lower average modulus measurement values in the contour plot. The degree-of-capability of this approach can be verified on its accurate identification and evaluation of the imperfections at the interphase. The indented area as shown in Fig. 7(a) contains a semisphere void imperfection that can be clearly identified in Fig. 7(b) using the results for the spatial variation of the modulus. It is worth mentioning that nanoindentation based measurements are considered as nondestructive measurements which adds a further advantage to the proposed experimental approach.

## 5 Conclusions

The localized viscoelastic properties such as shear creep compliance and Young's relaxation modulus at core–skin interphase of a sandwich composite were measured using a viscoelastic Berkovich nanoindentation technique. These measurements are necessary for the systematic characterization of sandwich composites at their interphase regions in order to improve their overall mechanical strength. The captured gradients (soft to hard) in the mechanical properties through the core–skin direction proves the effectiveness of this approach. Using the nanoindentation results, the time-averaged Young's modulus values were mapped on the

interphase indented area. A high correlation between the time-averaged Young's modulus mapping and the optical micrograph of the same indented area was obtained (e.g., hardening by fiber adhesion effects and softening due to imperfection were effectively captured). This agreement makes this mapping an effective tool to assess the core–skin interphase bonding quality of sandwich composites.

**Acknowledgements** We acknowledge the support of NSF WindStar I/UCRC Center (1362033) and also NSF CMMI-1661246, CMMI-1636306, and CMMI-1726435. We are also grateful to the constructive discussion with Mr. Nicholas Althoff and his colleagues at GE Renewable Energy. We thank DIAB, Hexion, and TPI Composites for supplying the core, resin, and glass materials, respectively used for the preparation of the composites. Lu is also grateful to the support by the Louis Beecherl Jr. Endowed Chair.



## References

Baumgaertel, M., Winter, H.H.: Determination of discrete relaxation and retardation time spectra from dynamic mechanical data. Rheol. Acta **28**, 511–519 (1989). https://doi.org/10.1007/BF01332922

Briscoe, B.J., Fiori, L., Pelillo, E.: Nano-indentation of polymeric surfaces. J. Phys. D, Appl. Phys. **31**, 2395–2405 (1998). https://doi.org/10.1088/0022-3727/31/19/006

Brøndsted, P., Lilholt, H., Lystrup, A.: Composite materials for wind power turbine blades. Annu. Rev. Mater. Res. **35**, 505–538 (2005). https://doi.org/10.1146/annurev.matsci.35.100303.110641

Cech, V., Palesch, E., Lukes, J.: The glass fiber-polymer matrix interface/interphase characterized by nanoscale imaging techniques. Compos. Sci. Technol. **83**, 22–26 (2013). https://doi.org/10.1016/j.compscitech.2013.04.014

Chen, Q., Linghu, T., Gao, Y., Wang, Z., Liu, Y., Du, R., Zhao, G.: Mechanical properties in glass fiber PVC-foam sandwich structures from different chopped fiber interfacial reinforcement through vacuum-assisted resin transfer molding (VARTM) processing. Compos. Sci. Technol. **144**, 202–207 (2017). https://doi.org/10.1016/j.compscitech.2017.03.033

Dai, J., Hahn, H.T.: Flexural behavior of sandwich beams fabricated by vacuum-assisted resin transfer molding. Compos. Struct. **61**, 247–253 (2003). https://doi.org/10.1016/S0263-8223(03)00040-0

Du, L., Jiao, G.: Indentation study of Z-pin reinforced polymer foam core sandwich structures. Composites, Part A, Appl. Sci. Manuf. **40**, 822–829 (2009). https://doi.org/10.1016/j.compositesa.2009.04.004

Emri, I., Tschoegl, N.W.: Generating line spectra from experimental responses. Part I: relaxation modulus and creep compliance. Rheol. Acta **32**, 311–322 (1993). https://doi.org/10.1007/BF00434195

Feng, G., Ngan, A.H.W.: Effects of creep and thermal drift on modulus measurement using depth-sensing indentation. J. Mater. Res. **17**, 660–668 (2002). https://doi.org/10.1557/JMR.2002.0094

Ferry, J.D.: Viscoelastic Properties of Polymers. Wiley, New York (1980)

Flores-Johnson, E.A., Li, Q.M.: Experimental study of the indentation of sandwich panels with carbon fibre-reinforced polymer face sheets and polymeric foam core. Composites, Part B, Eng. **42**, 1212–1219 (2011). https://doi.org/10.1016/j.compositesb.2011.02.013

Frostig, Y.: Behavior of delaminated sandwich beam with transversely flexible core—high order theory. Compos. Struct. **20**, 1–16 (1992). https://doi.org/10.1016/0263-8223(92)90007-Y

Gibson, R.F.: A review of recent research on nanoindentation of polymer composites and their constituents. Compos. Sci. Technol. **105**, 51–65 (2014). https://doi.org/10.1016/j.compscitech.2014.09.016

Huang, G.: Measurements of Viscoelastic Properties by Nanoindentation (2007). Stillwater

Huang, G., Lu, H.: Measurement of Young's relaxation modulus using nanoindentation. Mech. Time-Depend. Mater. **10**, 229–243 (2006). https://doi.org/10.1007/s11043-006-9020-3

Huang, G., Lu, H.: Measurements of two independent viscoelastic functions by nanoindentation. Exp. Mech. **47**, 87–98 (2007). https://doi.org/10.1007/s11340-006-8277-4

Jakes, J.E., Lakes, R.S., Stone, D.S.: Broadband nanoindentation of glassy polymers: part I. Viscoelasticity. J. Mater. Res. **27**, 463–474 (2012). https://doi.org/10.1557/jmr.2011.363

Knauss, W.G., Zhao, J.: Improved relaxation time coverage in ramp–strain histories. Mech. Time-Depend. Mater. **11**, 199–216 (2007). https://doi.org/10.1007/s11043-007-9035-4

Kucuk, Y., Mollamahmutoglu, C., Wang, Y., Lu, H.: Nonlinearly viscoelastic nanoindentation of PMMA under a spherical tip. Exp. Mech. **53**, 731–742 (2013). https://doi.org/10.1007/s11340-012-9695-0

Liu, C.K., Lee, S., Sung, L.P., Nguyen, T.: Load-displacement relations for nanoindentation of viscoelastic materials. J. Appl. Phys. **100** (2006). https://doi.org/10.1063/1.2220649

Lu, H., Wang, B., Ma, J., Huang, G., Viswanathan, H.: Measurement of creep compliance of solid polymers by nanoindentation. Mech. Time-Depend. Mater. **7**, 189–207 (2003). https://doi.org/10.1023/B:MTDM.0000007217.07156.9b

Ngan, A.H.W., Tang, B.: Viscoelastic effects during unloading in depth-sensing indentation. J. Mater. Res. **17**, 2604–2610 (2002). https://doi.org/10.1557/JMR.2002.0377

Ngan, A.H.W., Wang, H.T., Tang, B., Sze, K.Y.: Correcting power-law viscoelastic effects in elastic modulus measurement using depth-sensing indentation. Int. J. Solids Struct. **42**, 1831–1846 (2005). https://doi.org/10.1016/j.ijsolstr.2004.07.018

Oliver, W.C., Pharr, G.M.: An improved technique for determining hardness and elastic modulus using load and displacement sensing indentation experiments. J. Mater. Res. **7**, 1564–1583 (1992). https://doi.org/10.1557/JMR.1992.1564

Rizov, V., Shipsha, A., Zenkert, D.: Indentation study of foam core sandwich composite panels. Compos. Struct. **69**, 95–102 (2005). https://doi.org/10.1016/j.compstruct.2004.05.013

Sneddon, I.N.: The relation between load and penetration in the axisymmetric Boussinesq problem for a punch of arbitrary profile. Int. J. Eng. Sci. **3**, 47–57 (1965). https://doi.org/10.1016/0020-7225(65)90019-4

Stewart, R.: At the core of lightweight composites. Reinf. Plast. **53**, 30–35 (2009). https://doi.org/10.1016/S0034-3617(09)70112-2

Tschoegl, N.W., Emri, I., Emrl, I.: Generating line spectra from experimental responses. III. Interconversion between relaxation and retardation behavior. Int. J. Polym. Mater. **18**, 117–127 (1992). https://doi.org/10.1080/00914039208034818